

Dynamic Model-based Control of Redundantly Actuated, Non-holonomic, Omnidirectional Vehicles

Christoph Stöger, Andreas Müller and Hubert Gattringer

Institute of Robotics, Johannes Kepler University Linz, Altenberger Straße 69, 4040 Linz, Austria

Keywords: Dynamic Modeling and Control, Redundant Actuation, Pseudo-omnidirectional, Singularities.

Abstract: Vehicles with several centered orientable wheels have one of the highest maneuverability and are hence an excellent choice for transportation tasks in narrow environments. However, they are non-holonomic, in general redundantly actuated, and additionally suffer from configuration singularities, which makes their modeling and control challenging. Existing control approaches only consider the vehicle kinematics whereas the required torques are commonly controlled by classical PD motor controllers. However, this leads to considerable tracking errors and a violation of the constraints especially during acceleration phases. Moreover, actuator counteractions and an undefined torque distribution can be observed. This paper introduces a model-based control concept that overcomes these issues. It resolves counteractions and distributes torques according to physical limitations which significantly reduces slippage and the energy consumption and further reduces the tracking error. To this end, an inverse dynamics solution of a redundantly parametrized model is used. The method is robust to configuration singularities. This is confirmed by experimental results.

1 INTRODUCTION

Mobile platforms offer a large workspace for applications in service robotics as well as manufacturing. Their main application is, especially in industry, still the transportation of goods – a seemingly simple task that can, however, become very complex given the demand from industry for compact and cost-efficient shop floor solutions. A consequence is that a precise locomotion with a mobile base offering the maximum degree of maneuverability δ_M (Campion et al., 1996), i.e. $\delta_M = 3$, is ever more relevant. Vehicles with $\delta_M = 3$ are also called omnidirectional since they are able to move in each direction and independently change their orientation. Holonomic omnidirectional vehicles, equipped with $n \geq 3$ Mecanum or Swedish wheels, are the most popular type of this class. They need a small number of actuators, since they do not need to steer, and are easy to control. However, Mecanum wheels possess poor load capacities compared to standard wheels, they introduce vibrations to the actuators and chassis, and lead to much higher slippage. Platforms with $n \geq 2$ centered orientable standard wheels overcome these problems. Center orientable wheels are wheels which can be steered about a vertical axis passing through the center of the wheel. Such platforms are omnidirectional as well but

non-holonomic, i.e. they can independently attain any position and orientation but may have to reorient their wheels during the navigation. For this reason they are often called pseudo-omnidirectional.

The number of driven wheels depends on the transporter size, i.e. the payload, and is often higher than 2. The driving motors are thereby acting in parallel which means that the vehicle is not only non-holonomic but also redundantly actuated. There are several publications about the higher-level kinematic control of such vehicles (Giordano et al., 2009; Ofatadeh et al., 2013; Stöger et al., 2015), which results in a feasible motion of the wheels and moves the vehicle to a destination. However, there is hardly any lower-level dynamic control scheme for actually achieving this motion reported in the literature. It is mostly indicated that a simple PD controller is used. Such a control neither takes the dynamic of the vehicle into account, nor the redundancy of the actuation. Considerable errors in dynamic phases and unnecessary high torques due to the actuator counteraction, which again lead to slip, are the consequence.

Common approaches for controlling platforms with $\delta_M < 3$ can be divided into two classes: 1) robust control and 2) model-based control strategies. In the first class sliding mode controllers are widely used (Yang and Kim, 1999). One and the same controller

works for different loads quite well but the robustness has to be paid by a high switching frequency of the input torques. Thereby, the second class is more promising for us. A model-based inverse dynamics controller reduce the tracking error significantly and can easily be adapted if the load of the vehicle changes. So far there is hardly any dynamic control method for redundantly actuated platforms with $\delta_M = 3$. In (Lee and Li, 2015) the authors use the inverse dynamics solution extended by a sliding mode controller but have not addressed the redundancy resolution or counteraction avoidance. Methods for the control of redundantly actuated systems can be found in the field of parallel mechanisms (Müller and Hufnagel, 2012) and are adapted in this paper to the needs of mobile robots. Our aim is to use only a minimal demand of torque and to distribute this demand among the actuators by considering their limitations as well as differences in frictional conditions, e.g. due to an unbalanced load, in order to increase the uptime of the vehicle and reduce slippage in the resulting motion. The result is a novel concept for the low-level control of non-holonomic, omnidirectional vehicles equipped with an arbitrary number n of wheels. The control concept can be seen as building block which is independent from the higher-level control scheme used for motion planning.

Although there is a large number of dynamic models for other platform types, e.g. differential drives (Fukao et al., 2000) or car like systems (De Luca et al., 1998), only a few models are available for omnidirectional, non-holonomic vehicles. Moreover, those models either do not consider constraint forces (Lee and Li, 2015) or neglect the wheels (Ploeg et al., 2002) which results in a considerable model error. However, such models can still be found in the literature since they bypass the resolution of the singular rolling constraints. Therefore, a novel dynamic model is presented in this paper. It is redundantly parametrized, which is especially also valid in singular configurations, and includes all relevant effects. Constraining forces are numerically eliminated by a null space projection method (Müller and Hufnagel, 2012). The null space projector is computed by a novel semi-analytic orthogonalization method which takes the structure of the constraints into account and is computationally efficient. The latter is especially in the context of the control crucial.

The paper is structured as follows. In Section 2 the description of the platforms kinematics is presented. The configuration variables are described and the rolling constraints are formulated. In Section 3 the redundant parametrized dynamic model is derived whereby an overview about the modeled effects in-

cluding friction is given and the constraint forces are eliminated. In Section 4 the inverse dynamics is computed and the torque distribution method presented. Subsequently, the control concept is formulated and its asymptotic stabilization is proved. Experiments which validate the theory are presented in Section 5. The paper closes with a summary in Section 6 and some remarks for future research.

2 PLATFORM KINEMATICS

The variables that parametrize the current configuration of the platform, see Figure 1, can be divided into two sets (Ostrowski and Burdick, 1996). The first set describe the vehicle's posture, i.e. displacement of the chassis-fixed frame $\mathcal{F}_C = \{O_C, \mathbf{c}\mathbf{x}, \mathbf{c}\mathbf{y}\}$ relative to an inertial frame $\mathcal{F}_I = \{O_I, \mathbf{i}\mathbf{x}, \mathbf{i}\mathbf{y}\}$.

Assumption 1. *The vehicles motion is assumed to be restricted to the horizontal plane.*

With Assumption 1 the pose can be parametrized using $\mathbf{q}_C = (x, y, \gamma)^T \in SE(2)$. The vector $(x, y) \in \mathbb{R}^2$ describes the reference point O_C in the frame \mathcal{F}_I and $\gamma \in \mathcal{S}^1$ is the angle enclosed by $\mathbf{i}\mathbf{x}$ and $\mathbf{c}\mathbf{x}$.

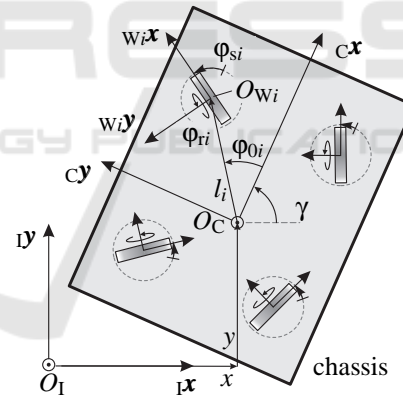


Figure 1: Non-holonomic, omnidirectional vehicle with $n = 4$ centered orientable wheels.

The second set of variables are called shape or internal variables. They describe the configuration of the locomotion system and are given by n roll angles φ_{ri} and n steer angles φ_{si} , with $i \in \{1, \dots, n\}$. They are summarized in

$$\mathbf{q}_\varphi = (\varphi_{r1}, \dots, \varphi_{rn}, \varphi_{s1}, \dots, \varphi_{sn})^T \in T^{2n}. \quad (1)$$

Here T^{2n} is the $2n$ dimensional torus. For later purpose additional frames $\mathcal{F}_{Wi} = \{O_{Wi}, \mathbf{w}_i\mathbf{x}, \mathbf{w}_i\mathbf{y}\}$ are attached at each drive unit.

The configuration of the mobile platform is thus described by the vector of generalized coordinates

$$\mathbf{q} = (\mathbf{q}_C^T, \mathbf{q}_\varphi^T)^T \in Q = SE(2) \times T^{2n}. \quad (2)$$

Although ideal rolling is a simplified assumption we can use it within the control in order to minimize the resultant slippage and counteraction. Ideal rolling means that the longitudinal velocity ($w_i \mathbf{x}$ direction) of a certain wheel i is consistent with its rolling speed, which requires

$$\cos(\varphi_{si} + \gamma)\dot{x} + \sin(\varphi_{si} + \gamma)\dot{y} + l_i \sin(\varphi_{si} - \varphi_{0i})\dot{\gamma} - r\dot{\varphi}_{ri} = 0, \quad (3)$$

and that the lateral velocity ($w_i \mathbf{y}$ direction) is zero, i.e.

$$-\sin(\varphi_{si} + \gamma)\dot{x} + \cos(\varphi_{si} + \gamma)\dot{y} + l_i \cos(\varphi_{si} - \varphi_{0i})\dot{\gamma} = 0. \quad (4)$$

The polar coordinates l_i and φ_{0i} describe the position of the i th wheel O_{W_i} observed from \mathcal{F}_C , see Figure 1.

The following properties directly follow from the rolling constraints, see Equation (3) and (4):

Property 1. *The constraints can be written in Pfaffian form, i.e. linear in velocities, as $\mathbf{J}(\mathbf{q})\dot{\mathbf{q}} = 0$.*

Property 2. *The n steering velocities $\dot{\varphi}_{si}$ are unconstrained. Hence, the columns of \mathbf{J} which correspond to them are zero.*

The rank m of $\mathbf{J} \in \mathbb{R}^{2n, 3+2n}$ determines the number of independent constraints. Hence, the number of independent velocities respecting the constraints, also referred to as generalized velocities, is

$$\delta_v = 3 + 2n - m. \quad (5)$$

Another interesting property is that the n lateral constraints (4) only restrict the chassis twist $(\dot{x}, \dot{y}, \dot{\gamma})$. By considering the corresponding rows in \mathbf{J} , one can easily proof the following property.

Property 3. *The number and set of independent lateral constraints depends on the steering angles and is between 1 and 3.*

In the case of $n > 2$ wheels the minimum number of generalized velocities is $\delta_v = 3 + 2n - (n + 3) = n$. Referring to Property 2, they are given by the unconstrained steering angles. In this case, the vehicle can not drive but only steer the wheels. Thus, vehicles with $n > 2$ wheels have to drive in regions of reduced rank. In this regions, only one particular twist, namely the rotation about the instantaneous center of rotation, is possible. Some wheel setups, especially for $n = 2$ wheels, permit the axial alignment of all wheel axes. In this special configuration, the number m of independent constraints further reduces by 1 since all lateral constraints are equal. Such configurations allow the vehicle to rotate about an arbitrary point on the line specified by the wheel axes. This is summarized by the following property.

Property 4. *The constraint matrix \mathbf{J} is either permanent singular or can become singular. The number of generalized velocities is thus $\delta_v \in \{n + 1, n + 2\}$.*

3 DYNAMIC MODELING

3.1 Redundantly Parametrized Equations of Motion

The equations of motion are derived using the *Projection Equations*

$$\sum_{b=1}^N \left[\frac{\partial \mathbf{R}\mathbf{v}_{c,b}}{\partial \dot{\mathbf{q}}} \quad \frac{\partial \mathbf{R}\boldsymbol{\omega}_b}{\partial \dot{\mathbf{q}}} \right]^T \begin{pmatrix} \mathbf{R}\dot{\mathbf{p}}_{c,b} + \mathbf{R}\tilde{\boldsymbol{\omega}}_{IR} \mathbf{R}\mathbf{p}_{c,b} - \mathbf{R}\mathbf{f}_{c,b} \\ \mathbf{R}\dot{\mathbf{L}}_b + \mathbf{R}\tilde{\boldsymbol{\omega}}_{IR} \mathbf{R}\mathbf{L}_b - \mathbf{R}\boldsymbol{\tau}_b \end{pmatrix} = 0. \quad (6)$$

Projection Equations are based on the *Newton-Euler equations* for body b which are evaluated in a reference frame \mathcal{F}_R , and are projected onto the direction of the generalized coordinates \mathbf{q} . Here $\mathbf{R}\mathbf{p}_{c,b} = m_b \mathbf{R}\mathbf{v}_{c,b}$ is the linear momentum of the center of gravity (c) of body b . $\mathbf{R}\mathbf{L}_b = \mathbf{R}\Theta_b \mathbf{R}\boldsymbol{\omega}_b$ is the angular momentum, and $\mathbf{R}\mathbf{v}_{c,b}$ and $\mathbf{R}\boldsymbol{\omega}_b$ are corresponding translational and angular velocities. $\tilde{\boldsymbol{\omega}}$ is a skew symmetric matrix representing the cross product $\tilde{\boldsymbol{\omega}}\mathbf{p} = \boldsymbol{\omega} \times \mathbf{p}$. $\mathbf{R}\mathbf{f}_{c,b}$ and $\mathbf{R}\boldsymbol{\tau}_b$ are total forces and torques acting on the center of gravity / body. The Equations (6) are used to model inertia effects, the influence of traction and friction forces as well as motor torques.

Inertia is considered for $N = 2n + 1$ bodies:

- the chassis (c)

and n drive units including:

- n steer motors (si), which are mounted on the chassis and are rigidly coupled with a drive unit
- n drive motors (ri), which are in turn mounted on the drive unit and are rigidly coupled with the wheel.

The inertia of the chassis is, in general, significantly higher than the inertia of the drive unit. However, since especially the orientation of the drive unit has a much higher acceleration they are relevant too. The velocities of the chassis are

$$\begin{aligned} {}_c\mathbf{v}_{c,c} &= (\dot{x} \cos(\gamma) + \dot{y} \sin(\gamma) \quad -\dot{x} \sin(\gamma) + \dot{y} \cos(\gamma) \quad 0)^T \\ {}_c\boldsymbol{\omega}_c &= (0 \quad 0 \quad \dot{\gamma})^T \end{aligned}$$

and the velocities of the steer axes and the rolling wheels are

$$\begin{aligned} w_i \mathbf{v}_{c,si} &= w_i \mathbf{v}_{c,ri} = \\ &\begin{pmatrix} \dot{x} \cos(\gamma + \varphi_{si}) + \dot{y} \sin(\gamma + \varphi_{si}) + l_i \sin(\varphi_{si} - \varphi_{0i})\dot{\gamma} \\ -\dot{x} \sin(\gamma + \varphi_{si}) + \dot{y} \cos(\gamma + \varphi_{si}) + l_i \cos(\varphi_{si} - \varphi_{0i})\dot{\gamma} \\ 0 \end{pmatrix} \end{aligned}$$

$$w_i \boldsymbol{\omega}_{si} = (0 \quad 0 \quad \dot{\gamma} + \dot{\varphi}_{si})^T$$

$$w_i \boldsymbol{\omega}_{ri} = (0 \quad \dot{\varphi}_{ri} \quad \dot{\gamma} + \dot{\varphi}_{si})^T,$$

all vectors are expressed in \mathcal{F}_{W_i} (Figure 1). It is assumed that the center of gravity of the drive unit coincides with the steering axis O_{W_i} .

There are two kinds of friction sources. The first kind is bearing friction. It is commonly modeled as a viscose and coulomb friction using a static model (Bona and Indri, 2005). The model is computationally inexpensive and the parameters can be easily identified since the model is linear w.r.t. the parameters. The second kind of friction source is the tire/soil contact. Since ideal rolling is assumed the generalized, i.e. projected, traction forces \mathbf{Q}_t are imposed by the constraints (3), (4):

$$\mathbf{Q}_t = \mathbf{J}^T \boldsymbol{\lambda}, \quad (7)$$

where $\boldsymbol{\lambda} \in \mathbb{R}^{2n}$ are the corresponding *Langrange multipliers*. The ground contact model must also take the rolling resistance into account. The rolling resistance is caused by elastic deformation of tire and soil, and can again be modeled (within a certain velocity range) by a Coulomb and viscous friction model (Hall and Moreland, 2001). The applied driving (r) and steering (s) torques are given by

$$\begin{aligned} w_i \boldsymbol{\tau}_{si} &= (0 \quad 0 \quad 1)^T (\tau_{si} - \mu_{sci} \text{sign}(\dot{\phi}_{si}) - \mu_{svi} \dot{\phi}_{si}) \\ w_i \boldsymbol{\tau}_{ri} &= (0 \quad 1 \quad 0)^T (\tau_{ri} - \mu_{rci} \text{sign}(\dot{\phi}_{ri}) - \mu_{rvi} \dot{\phi}_{ri}), \end{aligned}$$

where μ are friction coefficients for the Coulomb (c) and viscous (v) friction, τ_{si} is the steering torque and τ_{ri} the rolling torque, respectively. The discontinuous $\text{sign}(x)$ function leads to chattering about zero velocity. In order to avoid that, this function is replaced in the control law by the smooth $\tanh(x/\varepsilon)$ function. The parameter ε is used to determine the region where the force is reduced due to low speeds. The value of ε depends on the application. In the experiment it was set to 0.01 rad/s, which corresponds to a driving speed of ≈ 1 mm/s for the considered system.

The dynamics of the non-holonomic, omnidirectional vehicle can be expressed by the system of differential algebraic equations

$$\mathbf{M}(\mathbf{q})\ddot{\mathbf{q}} + \mathbf{C}(\mathbf{q}, \dot{\mathbf{q}})\dot{\mathbf{q}} + \mathbf{f}(\dot{\mathbf{q}}) = \mathbf{B}(\mathbf{q})\mathbf{u} + \mathbf{J}(\mathbf{q})^T \boldsymbol{\lambda} \quad (8a)$$

$$\mathbf{J}(\mathbf{q})\dot{\mathbf{q}} = 0. \quad (8b)$$

Here $\mathbf{M} \in \mathbb{R}^{2n+3, 2n+3}$ is the generalized inertia matrix, $\mathbf{C}\dot{\mathbf{q}} \in \mathbb{R}^{2n+3}$ includes Coriolis and centrifugal forces, $\mathbf{f} \in \mathbb{R}^{2n+3}$ Coulomb and viscous friction, $\mathbf{u} = (\tau_{r1}, \dots, \tau_{rn}, \tau_{s1}, \dots, \tau_{sn}) \in \mathbb{R}^{2n}$, and $\mathbf{B} \in \mathbb{R}^{2n+3, 2n}$ are the input torques and matrix, and $\mathbf{J}^T \boldsymbol{\lambda}$ the generalized constraining forces acting on the system.

Assumption 2. *It is assumed that each wheel is fully actuated, i.e. each wheel has a steering and driving motor.*

Then, the input matrix has the following structure

$$\mathbf{B} = \begin{bmatrix} \mathbf{B}_r & \mathbf{0}_{n+3, n} \\ \mathbf{0}_{n, n+3} & \mathbf{I}_{n, n} \end{bmatrix} \quad (9)$$

where $\mathbf{0}_{i, j} \in \mathbb{R}^{i, j}$ is a zero matrix, $\mathbf{I}_{n, n} \in \mathbb{R}^{n, n}$ a identity matrix and

$$\mathbf{B}_r = \begin{bmatrix} \mathbf{0}_{3, n} \\ \mathbf{I}_{n, n} \end{bmatrix}. \quad (10)$$

The dimensions slightly change for vehicles where this is not the case but the method is still valid.

3.2 Elimination of Constraint Forces

The Equations (8) form a differential algebraic system, and their evaluation requires the determination of the Lagrange multipliers $\boldsymbol{\lambda}$. The computational expense of this computation is in particular problematic since it should be used within the control law (Müller and Hufnagel, 2012). Therefore, the constraint reactions are not computed but eliminated instead. This is commonly done by reformulating the equations of motion with a set of generalized velocities that respect the constraints. However, the subset of regular constraints depends on the configuration of the vehicle. As a consequence, a set of different generalized velocities and their corresponding dynamics equations are often used. However, this leads to issues during the transition between these models which can be avoided by the following approach.

(Müller and Hufnagel, 2012) suggest to use one redundantly parametrized model, as in (8), but eliminate the constraining forces by projecting the dynamics equation with a projector \mathbf{N} to the null space of \mathbf{J} . This projector is not unique. The requirements are

$$\mathbf{J}\mathbf{N} = 0, \quad (11)$$

i.e. \mathbf{N} is an orthogonal complement of \mathbf{J} , and $\text{rank}(\mathbf{N}) = \delta_v$, i.e. \mathbf{N}^T only removes constraining forces. Projecting Equations (8) leads to

$$\mathbf{N}^T (\mathbf{M}\ddot{\mathbf{q}} + \mathbf{C}\dot{\mathbf{q}} + \mathbf{f}) = \mathbf{N}^T \mathbf{B}\mathbf{u}. \quad (12)$$

There are two methods proposed by (Müller and Hufnagel, 2012) for the analytic computation of \mathbf{N} . Both, however assume regular constraints and, as a consequence of Property 4, are not directly applicable for pseudo-omnidirectional vehicles. In this work a semi-analytical approach is used which consist of an analytical and a numerical step.

In the *analytical* step Property 2 is used to determine n columns of \mathbf{N} . The columns $k \in \{4 + n, \dots, 3 + 2n\}$, corresponding to the steering velocities, of \mathbf{J} are zero. Hence, unit vectors \mathbf{u}_k , which are zero but have 1 at the k th component, lie in the null space of the

Algorithm 1: Gram-Schmidt inspired projection method for the null space computation. $\|\cdot\|$ is the Euclidean vector norm.

```

1 Function compute_remaining_null_space_vectors
   input : Constraint matrix  $\mathbf{J}$ 
   output: Remaining null space directions  $\mathbf{N}_n$ 
2    $\mathbf{K} = [\mathbf{J}^T]$ ,  $\mathbf{N}_n = []$ ,  $i = 1$ 
3    $\delta_v = n$ 
4   for  $i = 1, \dots, 3$  do
5      $\dot{\mathbf{q}} = \mathbf{u}_i$ 
6      $i = i + 1$ 
7     eliminate_directions( $\dot{\mathbf{q}}$ ,  $\mathbf{K}$ )
8     if  $\|\dot{\mathbf{q}}\| > \varepsilon$  then
9        $\dot{\mathbf{q}} = \dot{\mathbf{q}} / \|\dot{\mathbf{q}}\|$ 
10       $\mathbf{N}_n = [\mathbf{N}_n, \dot{\mathbf{q}}]$ 
11       $\delta_v = \delta_v + 1$ 
12       $\mathbf{K} = [\mathbf{K}, \dot{\mathbf{q}}]$ 
13    end
14  end
15 end
16 Function eliminate_directions
   input :  $\dot{\mathbf{q}}$  vector under consideration,  $\mathbf{K}$  column
           vectors represent directions which
           should be eliminated
   output:  $n$ : remaining components of  $\dot{\mathbf{q}}$ 
17   $k = 1$ 
18  repeat
19     $\mathbf{j} = \text{column}(\mathbf{K}, k)$ 
20     $k = k + 1$ 
21     $\dot{\mathbf{q}} = \dot{\mathbf{q}} - \left( \frac{\dot{\mathbf{q}}^T \mathbf{j}}{\|\mathbf{j}\|^2} \right) \mathbf{j}$ 
22  until  $\|\dot{\mathbf{q}}\| < \varepsilon$  or  $k > nr\_of\_columns(\mathbf{K})$ 
23 end
    
```

constraint Jacobian, i.e. $\mathbf{J}\mathbf{u}_k = 0$. Hence, the full rank matrix

$$\mathbf{N}_a = \begin{bmatrix} \mathbf{0}_{n+3,n} \\ \mathbf{I}_{n,n} \end{bmatrix} \quad (13)$$

satisfies (11). This provides n columns of \mathbf{N} .

In the *numerical* step the remaining $\delta_v - n$ null space vectors are computed. This is commonly done by a singular value or full QR decomposition. These algorithms, however, compute a basis for both, the $n + 2$ (or $n + 1$) constrained and the remaining 1 (or 2) unconstrained directions and thereby add an unnecessary high computational expense to the methodology. An algorithm that avoids this is introduced in the following, see Algorithm 1. It is inspired by the *Gram-Schmidt* orthogonalization (Björck, 1994).

The algorithm determines a non-trivial vector $\dot{\mathbf{q}}_r$, which is orthogonal to the constrained directions \mathbf{j} , where \mathbf{j} is a transposed row of \mathbf{J} and hence again fulfills $\mathbf{J}\dot{\mathbf{q}}_r = 0$. The search starts with $\dot{\mathbf{q}} = \mathbf{u}_1 = (1, 0, \dots, 0)^T$ that correspond to a pure translation in the x -direction of frame \mathcal{F}_1 , see Figure 1 and (2). The rolling constraints are obviously violated since the entries that correspond to the drive velocities ϕ_{ri} are

zero. However, since the column space of \mathbf{J}^T and the allowed directions form an orthogonal complement, this vector can always be split into allowed and constrained components. The constrained components are removed in the *elimination_directions* phase by means of a vector projection. This reveals whether there is any motion possible which has a component in the x -direction. If not, the y -direction or finally a pure rotation is tried. The algorithm also works in the case of aligned wheel axes, i.e. 2 missing vectors. The only thing to do is to continue searching after one admissible velocity is found, and to remove not only the constrained directions but also the former found admissible directions.

The computation is very efficient since the projection, which is needed for the elimination step, only consists of simple arithmetical operations and the number of projections is limited to $6n$. \mathbf{J} has only zero columns in the last n entries, thus the result has the following structure

$$\mathbf{N}_n = \begin{bmatrix} \mathbf{N}_r \\ \mathbf{0}_{n, \delta_v - n} \end{bmatrix} \quad (14)$$

where $\mathbf{N}_r \in \mathbb{R}^{n+3, \delta_v - n}$ is computed by the algorithm, so that the columns of \mathbf{N}_r are orthonormal.

Combining the analytical \mathbf{N}_a and numerical \mathbf{N}_n null space bases finally result in

$$\mathbf{N} = [\mathbf{N}_n \quad \mathbf{N}_a] = \begin{bmatrix} \mathbf{N}_r & \mathbf{0}_{n+3,n} \\ \mathbf{0}_{n, \delta_v - n} & \mathbf{I}_{n,n} \end{bmatrix}. \quad (15)$$

Property 5. *The columns of the null space projection matrix \mathbf{N} are orthonormal. Hence the left inverse of \mathbf{N} is given by its transposed.*

4 MODEL-BASED CONTROL

4.1 Inverse Dynamics and Redundancy Resolution

At this point the inverse dynamics can be computed by evaluating (12) with a desired motion $\mathbf{q}_d(t)$

$$\mathbf{N}^T \mathbf{M} \ddot{\mathbf{q}}_d + \mathbf{N}^T \mathbf{C} \dot{\mathbf{q}}_d + \mathbf{N}^T \mathbf{f} = \mathbf{Q}_d = \mathbf{N}^T \mathbf{B} \mathbf{u}_{ID}, \quad (16)$$

which determines the required generalized forces \mathbf{Q}_d . Resolving the last term in (16) yields required torques \mathbf{u}_{ID} thus solving the inverse dynamics problem. The computational effort of this task can be significantly reduced if the structures of \mathbf{B} , see (9), and \mathbf{N} , see (15), are taken into account

$$\begin{bmatrix} \mathbf{N}_r^T \mathbf{B}_r & \mathbf{0}_{\delta_v - n, n} \\ \mathbf{0}_{n, n+3} & \mathbf{I}_{n, n} \end{bmatrix} \begin{pmatrix} \mathbf{u}_r \\ \mathbf{u}_s \end{pmatrix} = \begin{pmatrix} \mathbf{Q}_{r,d} \\ \mathbf{Q}_{s,d} \end{pmatrix}. \quad (17)$$

Hence, the special choice of \mathbf{N} decouples the driving \mathbf{u}_r and steering \mathbf{u}_s torques. The latter are directly given by the last n elements $\mathbf{Q}_{s,d}$ of the generalized torques \mathbf{Q}_d .

The driving torques must be computed by the remaining equations

$$\bar{\mathbf{B}}_r \mathbf{u}_r = \mathbf{Q}_{r,d}. \quad (18)$$

By investigating the dimensions of the projected input matrix $\bar{\mathbf{B}}_r = \mathbf{N}_r^T \mathbf{B}_r \in \mathbb{R}^{\delta_v - n, n}$, where $\delta_v - n$ is in general 1 or 2, it follows that the equation is underdetermined. Hence, there is an infinity number of driving torques \mathbf{u}_r which result in the same $\mathbf{Q}_{r,d}$. The system is therefore called redundantly actuated. To resolve this redundancy, the solution is chosen which minimize the following quadratic cost function (Müller, 2011)

$$\mathbf{u}_r^* = \arg \min_{\mathbf{u}_r} \frac{1}{2} \mathbf{u}_r^T \mathbf{W} \mathbf{u}_r \quad (19a)$$

$$\text{s.t. } \bar{\mathbf{B}}_r \mathbf{u}_r = \mathbf{Q}_{r,d}, \quad (19b)$$

with a positive definite weight matrix $\mathbf{W} \in \mathbb{R}^{n,n}$. The cost function ensures that only a minimal torque demand is used to provide $\mathbf{Q}_{r,d}$. The distribution of this demand can be done by choosing a proper weight matrix. In our approach the following diagonal matrix is used

$$\mathbf{W} = \text{diag} (1/\tau_{r,\max 1}^2, \dots, 1/\tau_{r,\max n}^2), \quad (20)$$

whereby $\tau_{r,\max i}$ are the maximum torques w.r.t. the motor and friction limitations. The latter is approximated by the stall torques, that is the maximum torque which can be applied to a single wheel, while accelerating the chassis against a stop, that does not result in slippage. They are determined by experiments and should include frictional differences due to an unbalanced load in the torque distribution.

The solution of (19) is given by

$$\mathbf{u}_r = \underbrace{\mathbf{W}^{-1} \bar{\mathbf{B}}_r^T (\bar{\mathbf{B}}_r \mathbf{W}^{-1} \bar{\mathbf{B}}_r^T)^{-1}}_{=: \bar{\mathbf{B}}_r^+} \mathbf{Q}_{r,d}. \quad (21)$$

Where $\bar{\mathbf{B}}_r^+$ is a right inverse of $\bar{\mathbf{B}}_r$, i.e. $\bar{\mathbf{B}}_r \bar{\mathbf{B}}_r^+ = \mathbf{I}_{n,n}$.

Summarizing, the inverse dynamics yields

$$\mathbf{u}_{ID} = (\mathbf{N}^T \mathbf{B})^+ \mathbf{Q}_d, \quad (22)$$

with the right inverse

$$(\mathbf{N}^T \mathbf{B})^+ = \begin{bmatrix} \bar{\mathbf{B}}_r^+ & \mathbf{0}_{l-n,n} \\ \mathbf{0}_{n,n+3} & \mathbf{I}_{n,n} \end{bmatrix} \quad (23)$$

of the projected input matrix $\mathbf{N}^T \mathbf{B}$.

4.2 Augmented PD-control

The inverse dynamics (22) provides the torque needed to follow a given desired motion \mathbf{q}_d . However, there is no feedback stabilization mechanism in this law. Hence, model uncertainties and disturbances will inevitably lead to significant errors. The classical approach to eliminate these errors is a decentralized strategy which independently controls the $2n$ actuated degrees of freedom

$$\tau_{ri} = P_r \int_0^t (\dot{\phi}_{ri,d} - \dot{\phi}_{ri}) d\tau + D_r (\dot{\phi}_{ri,d} - \dot{\phi}_{ri}) \quad (24)$$

$$\tau_{si} = P_s (\phi_{si,d} - \phi_{si}) + D_s (\dot{\phi}_{si,d} - \dot{\phi}_{si}). \quad (25)$$

The rolling constraints instantaneously only admit $\delta_v \in \{n+1, n+2\}$ independent velocities, hence the result is a violation of the rolling constraints and a counteraction of the control torques.

Our approach resolves this problem by a centralized model-based control

$$\mathbf{u}_{APD} = (\mathbf{N}^T \mathbf{B})^+ \left(\mathbf{N}^T \mathbf{M} \ddot{\mathbf{q}}_d + \mathbf{N}^T \mathbf{C} \dot{\mathbf{q}}_d + \mathbf{N}^T \mathbf{f} + \mathbf{D} \mathbf{N}^T (\dot{\mathbf{q}}_d - \dot{\mathbf{q}}) + \mathbf{P} \int_0^t \mathbf{N}^T (\dot{\mathbf{q}}_d - \dot{\mathbf{q}}) d\tau \right). \quad (26)$$

The system matrices and vectors $\mathbf{M}, \mathbf{C}, \mathbf{f}$ are evaluated by the vehicles current pose/velocity. The arguments of them are suppressed due to the lack of space. $\mathbf{D}, \mathbf{P} \in \mathbb{R}^{\delta_v, \delta_v}$ are positive definite gain matrices. The idea behind (26) is to use the projected velocity error and its integral

$$\mathbf{e}_v = \mathbf{N}^T (\dot{\mathbf{q}}_d - \dot{\mathbf{q}}), \quad \mathbf{e}_p = \int_0^t \mathbf{e}_v d\tau, \quad (27)$$

instead of the individual velocity error of each wheel to stabilize the system. The counteraction is thereby removed since the dimension of the error is equal to the local degree of freedom δ_v . The resulting torques are finally again distributed in a minimal fashion over the existing drives.

In the following it is proven that (26) asymptotically stabilizes $\dot{\mathbf{q}}$ along a desired motion $\dot{\mathbf{q}}_d$. It is therefore assumed that the desired velocity $\dot{\mathbf{q}}_d$ is provided by a higher-level controller and respects the constraints. By applying (26) to (12) and project it into unconstrained directions, the closed loop dynamic equations can be formulated as follows

$$\mathbf{N}^T \mathbf{M} (\ddot{\mathbf{q}}_d - \ddot{\mathbf{q}}) + \mathbf{N}^T \mathbf{C} (\dot{\mathbf{q}}_d - \dot{\mathbf{q}}) + \mathbf{D} \mathbf{e}_v + \mathbf{P} \mathbf{e}_p = \mathbf{0}. \quad (28)$$

Moreover, $\dot{\mathbf{q}}$ and $\dot{\mathbf{q}}_d$ respect the constraints. Hence, they are lying in the null space of \mathbf{J} and, as such, can be expressed by a linear combination $\mathbf{v}_1, \mathbf{v}_2$ of the basis \mathbf{N} of this space

$$\dot{\mathbf{q}}_d - \dot{\mathbf{q}} = \mathbf{N} \mathbf{v}_1 - \mathbf{N} \mathbf{v}_2 = \mathbf{N} \mathbf{e}_v. \quad (29)$$

It follows from Property 5 and Equation (27) that $\mathbf{e}_v = \mathbf{v}_1 - \mathbf{v}_2$. Inserting (29) in (28), yields the following error system

$$\tilde{\mathbf{M}}\dot{\mathbf{e}}_v + \tilde{\mathbf{C}}\mathbf{e}_v + \mathbf{D}\mathbf{e}_v + \mathbf{P}\mathbf{e}_p = 0 \quad (30)$$

with the projected mass matrix $\tilde{\mathbf{M}} = \mathbf{N}^T \mathbf{M} \mathbf{N}$ and the projected Coriolis and centrifugal forces $\tilde{\mathbf{C}}\mathbf{e}_v$ where $\tilde{\mathbf{C}} = \mathbf{N}^T \mathbf{M} \dot{\mathbf{N}} + \mathbf{N}^T \mathbf{C} \mathbf{N}$. The stability can be proven by introducing the following *Lyapunov function*

$$V = \frac{1}{2} \mathbf{e}_v^T \tilde{\mathbf{M}} \mathbf{e}_v + \frac{1}{2} \mathbf{e}_p^T \mathbf{P} \mathbf{e}_p. \quad (31)$$

Differentiating V w.r.t. time along a solution $\mathbf{e}_v(t), \mathbf{e}_p(t)$ of (30) yields

$$\dot{V} = \frac{1}{2} \mathbf{e}_v^T (\tilde{\mathbf{M}} - 2\tilde{\mathbf{C}}) \mathbf{e}_v - \mathbf{e}_v^T \mathbf{D} \mathbf{e}_v = -\mathbf{e}_v^T \mathbf{D} \mathbf{e}_v \leq 0. \quad (32)$$

Thereby, the following properties are used:

Property 6. $\tilde{\mathbf{M}}$ is positive definite,

Property 7. $\tilde{\mathbf{M}} - 2\tilde{\mathbf{C}}$ is skew symmetric.

The proof of them can be found in (Murray et al., 1994). Referring to the *Krasovskii-LaSalle invariance principle*, for a positive definite function $V > 0$ with a negative semi-definite derivative $\dot{V} \leq 0$ the state converge to a rest position in the subset of $\dot{V} = 0$. The only rest position of (30) in this subset is $(\mathbf{e}_v(t), \mathbf{e}_p(t)) = (0, 0)$ which proves the asymptotic stabilization of the control law.

5 EXPERIMENTAL RESULTS

In this Section experimental results of the proposed theory are presented. The used vehicle is equipped with $n = 2$ actuated wheels and is shown in Figure 2. The wheels are diametrically mounted about the reference point O_C . The front wheel is indexed by $i = 1$, the rear wheel by $i = 2$. The driving motors are DC motors with a maximum torque of 25.6Nm. They allow a maximum driving speed of 4.1rad/s which equals a linear velocity of $\dot{\varphi}_i r = 0.41$ m/s with a wheel radius $r = 0.1$ m. The steering motors are brushless DC motors with a maximum torque of 129Nm and a maximum steering speed of 195.95°/s. Selected parameters of the considered vehicle are summarized in Table 1.

Figure 3 visualizes the driven maneuver. It can be divided into two parts. The first part ($t = 0 \dots 5$ s) is a pure rotation by $\gamma = 180^\circ$ about the reference point O_C . Therefore, the wheel axes have to be aligned, hence it is a motion where the constraints are singular. In the second part, a mixed motion with translational and rotational components is done in a regular



Figure 2: Non-holonomic omnidirectional manipulator with $n = 2$ actuated wheels. The laser scanner marks the front side.

Table 1: Selected parameters of the equations of motion. Inertias are given together with the corresponding rotation axes.

symbol	value	description
m_C	93 kg	chassis weight
C_C	4.51 kg m ²	inertia chassis w _i z axis
B_i	20.5 · 10 ⁻³ kg m ²	inertia steering unit w _i y
C_i	0.2234 kg m ²	inertia steering unit w _i z
μ_{rci}	0.88 Nm	Coulomb, driving
μ_{rvi}	0.35 Nm s/rad	viscous, driving
μ_{sci}	2.11 Nm	Coulomb, steering
μ_{svi}	2.08 Nm s/rad	viscous, steering

configuration. The orientation is chosen to be always tangential to the desired (x_d, y_d) curve. The corresponding steering and driving velocities are summarized in Figure 4. The motion is firstly controlled by a classic PD control approach (25) and secondly by the proposed model-based control (26). A fair comparison between them is ensured by an independent optimization of the corresponding control coefficients. The result of this optimization is summarized in Table 2. The coefficients P_r and D_r corresponds to the error component which is projected by \mathbf{N}_r while P_s and D_s correspond to the projection of \mathbf{N}_s .

Since the steering angles are unconstrained and regularly actuated, both control concepts result in the same error correction laws. Thus, the same control coefficients can be used. Differences between the resulting tracking errors, see Figure 6, are a result of the inverse dynamics and can be primary seen in acceleration phases $t \in \{11, 15, \dots, 18\}$ s. There, the model-based control result in a significantly lower tracking error. The tracking error of the driving velocities can

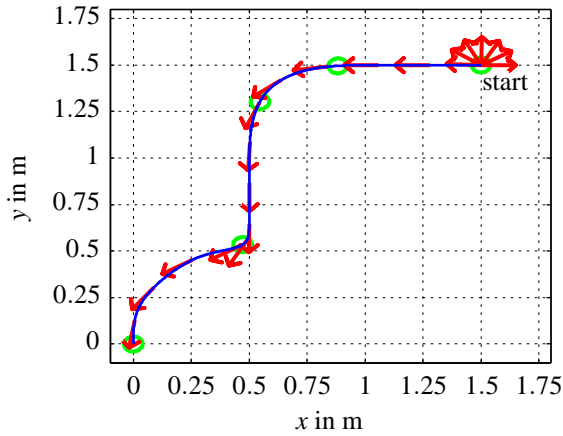


Figure 3: — Desired chassis position, ← sampled chassis orientation and driving direction, ○ points in time $t_i \in \{0s, 10s, 12s, 16s, 22s\}$.

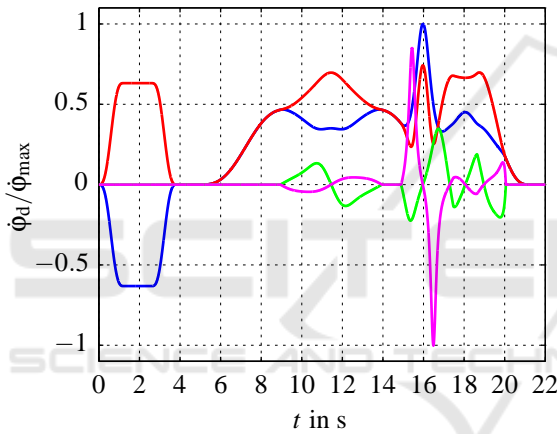


Figure 4: Driving velocity of — front and — rear wheel normalized by $r\dot{\phi}_{r,max} = 0.4m/s$, steering velocity of — front and — rear wheel normalized by $\dot{\phi}_{s,max} = 180^\circ/s$.

be found for the front wheel $i = 1$ in Figure 5. Significant differences can again mainly be found at acceleration phases $t \in \{0, 3, 16, 20\}s$. The differences can also be seen in the total slip distance (constraint violation)

$$\Delta_i = \int_{t=0}^T \sqrt{\dot{\Delta}_{longi}^2 + \dot{\Delta}_{lati}^2} dt. \quad (33)$$

It is computed by integrating the left-hand side of Equation (3) and (4). Due to violation they are not zero but equal to some longitudinal $\dot{\Delta}_{longi}$ and lateral $\dot{\Delta}_{lati}$ slip. Along the 2.595m long path, the model-based control leads to $\Delta_1 + \Delta_2 = 0.041m$ (1.58% of total path length) slip distance, whereby classic PD control leads $\Delta_1 + \Delta_2 = 0.137m$ (5.28% of total path length) slip distance.

Significant differences can also be noticed in the

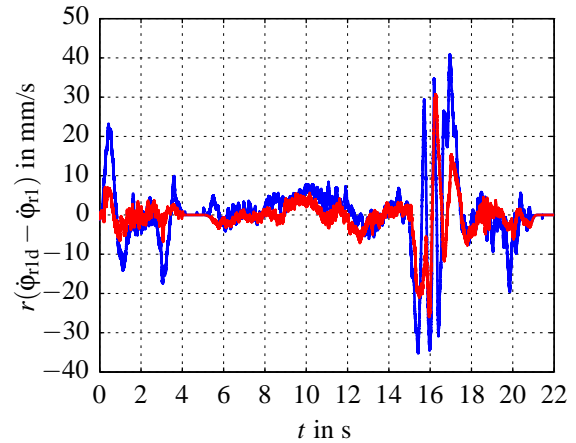


Figure 5: Velocity tracking error for the — classic PD and — model-based controlled front wheel $i = 1$.

Table 2: Control coefficients.

symbol	value	description
P_r	0.937 Nm/rad	driving classic
D_r	0.181 Nm s/rad	driving classic
P_r	0.112 Nm/rad	driving model-based
D_r	0.238 Nm s/rad	driving model-based
P_s	1.13 Nm/rad	steering
D_s	0.3 Nm s/rad	steering
$\tau_{r,max1}$	9.6 Nm	torque weight front
$\tau_{r,max2}$	10.2 Nm	rear motor

resulting driving torques. They are presented for the classic control in Figure 7 and for the model-based PD control in Figure 8. Between $t = 10s$ and $12s$ it can be seen that the classic control result in significant higher driving torques than the model-based approach. Moreover, the torques show an opposite sign. Hence, one motor is accelerating while the other decelerates. This is a clear result of the counteraction and an arbitrary distribution of the torque demand. Further investigations show, that this higher demand can be observed over the whole trajectory. As indicator for the energy demand, the quadratic average of the torques is used

$$\bar{\tau}^2 = \frac{1}{T} \int_{t=0}^T \tau^2 dt. \quad (34)$$

For the model-based control this indicator is $\bar{\tau}_{r1} + \bar{\tau}_{r2} = 3.039Nm$ which is 14.75% lower than the 3.565Nm for the classic control. The consequence is a much lower energy demand for the model-based control, and as a result a much higher uptime.

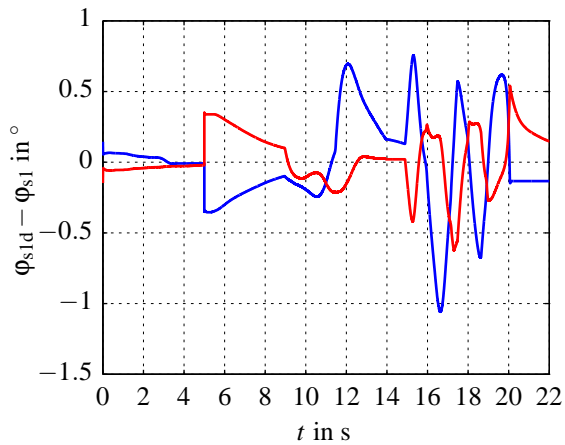


Figure 6: Steering tracking error for the — classic PD and — model-based controlled front wheel $i = 1$.

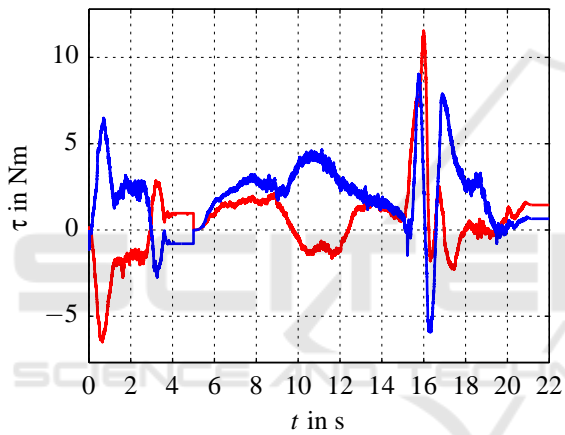


Figure 7: Driving torque for the classic DP control. — Front wheel $i = 1$ and — rear wheel $i = 2$.

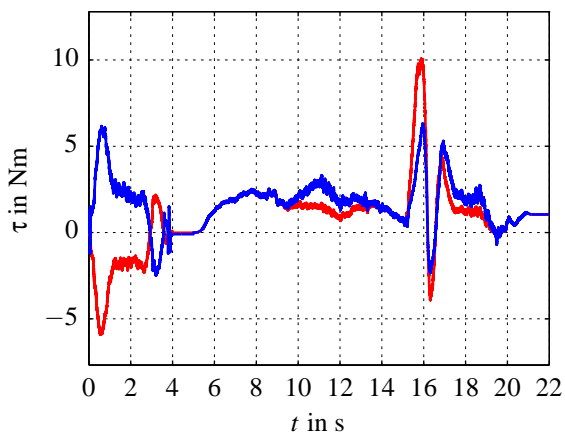


Figure 8: Driving torque for the model-based control. — Front wheel $i = 1$ and — rear wheel $i = 2$.

6 SUMMARY AND OUTLOOK

In this work a model-based dynamic control concept is introduced for redundantly actuated, non-holonomic and omnidirectional vehicles with n centered orientable standard wheels.

The first part of this paper introduces a framework for the dynamic modeling of such vehicles, including friction and inertia effects. It turned out, that the kinematic constraints of the vehicle are permanently singular or can become singular. Therefore the dynamics is modeled with a redundant set of coordinates. This formulation does not eliminate unknown traction forces (constraint forces) in the dynamic equations but is in each configuration, especially in singular configurations, valid. The elimination of the constraint forces is done through projecting the dynamics equation with a null space projector of the constraints. This projector is computed in a highly efficient manner by a semi-analytical approach.

The second part uses this model for an augmented PD-control consisting of an inverse dynamics component as well as a stabilizing feedback PD control law. The distribution of the computed torque among the different actuators is done through a weighted least square approach. Whereby wheels with a higher stall torque, which is the maximum motor torque that does not result in slippage, during accelerating the chassis against a mechanical stop, are less weighted. A PD control is additionally used to asymptotically stabilize the vehicle along a desired motion. The counteraction is thereby avoided by using the projected velocity error instead of the individual wheel velocity errors.

Future work will focus on the online identification of the load weight and the frictional conditions. This knowledge can be used to adapt the parameters of the inverse dynamics as well as the torque balancing law which improves the robustness of the concept. Additionally, the dynamic model will be used to monitor the vehicles state enabling a higher-level logic to detect faults on the drive units and unexpected collisions.

ACKNOWLEDGEMENTS

This work has been supported by the Austrian COMET-K2 program of the Linz Center of Mechatronics (LCM), and was funded by the Austrian federal government and the federal state of Upper Austria.

REFERENCES

- Björck, Å. (1994). Numerics of gram-schmidt orthogonalization. *Linear Algebra and Its Applications*, 197:297–316.
- Bona, B. and Indri, M. (2005). Friction compensation in robotics: an overview. In *Conference on Decision and Control and European Control Conference*, pages 4360–4367. IEEE.
- Campion, G., Bastin, G., and D'Andréa-Novel, B. (1996). Structural properties and classification of kinematic and dynamic models of wheeled mobile robots. *Transactions on Robotics and Automation*, 12:47–62.
- De Luca, A., Oriolo, G., and Samson, C. (1998). Feedback control of a nonholonomic car-like robot. In *Robot motion planning and control*, pages 171–253. Springer.
- Fukao, T., Nakagawa, H., and Adachi, N. (2000). Adaptive tracking control of a nonholonomic mobile robot. *Robotics and Automation, IEEE Transactions on*, 16(5):609–615.
- Giordano, P. R., Fuchs, M., Albu-Schäffer, A., and Hirzinger, G. (2009). On the kinematic modeling and control of a mobile platform equipped with steering wheels and movable legs. In *International Conference on Robotics and Automation*, pages 4080–4087. IEEE.
- Hall, D. E. and Moreland, J. C. (2001). Fundamentals of rolling resistance. *Rubber chemistry and technology*, 74(3):525–539.
- Lee, M.-H. and Li, T.-H. S. (2015). Kinematics, dynamics and control design of 4wis4wid mobile robots. In *The Journal of Engineering*, volume 1. IET.
- Müller, A. (2011). A robust inverse dynamics formulation for redundantly actuated pkm. In *13th World Congress in Mechanism and Machine Science, Guanajuato, Mexico*, pages 19–25.
- Müller, A. and Hufnagel, T. (2012). Model-based control of redundantly actuated parallel manipulators in redundant coordinates. *Robotics and Autonomous Systems*, 60(4):563–571.
- Murray, R. M., Li, Z., Sastry, S. S., and Sastry, S. S. (1994). *A mathematical introduction to robotic manipulation*. CRC press.
- Oftadeh, R., Ghabcheloo, R., and Mattila, J. (2013). A novel time optimal path following controller with bounded velocities for mobile robots with independently steerable wheels. In *International Conference on Intelligent Robots and Systems*, pages 4845–4851. IEEE.
- Ostrowski, J. and Burdick, J. (1996). Geometric perspectives on the mechanics and control of robotic locomotion. In *Robotics Research*, pages 536–547. Springer.
- Ploeg, J., van der Knaap, A. C., Verburg, D. J., and Automotive, T. (2002). Design, implementation and evaluation of a high performance agv. In *Intelligent Vehicle Symposium*. IEEE.
- Stöger, C., Müller, A., and Gattringer, H. (2015). Kinematic analysis and singularity robust path control of a non-holonomic mobile platform with several steerable driving wheels. In *International Conference on Intelligent Robots and Systems*, pages 4140–4145. IEEE.
- Yang, J.-M. and Kim, J.-H. (1999). Sliding mode control for trajectory tracking of nonholonomic wheeled mobile robots. *Robotics and Automation, IEEE Transactions on*, 15(3):578–587.